Similarity renormalization group with novel generators

W. Li, E. R. Anderson, and R. J. Furnstahl

The Similarity Renormalization Group with Novel Generators

W. Li,[*] E.R. Anderson,[†] and R.J. Furnstahl[‡]

Department of Physics, The Ohio State University, Columbus, OH 43210

The choice of generator in the Similarity Renormalization Group (SRG) flow equation determines the evolution pattern of the Hamiltonian. The kinetic energy has been used in the generator for most prior applications to nuclear interactions with other options largely unexplored. Here we show how variations of this standard choice can allow the evolution to proceed more efficiently without losing its advantages.

I. INTRODUCTION

The Similarity Renormalization Group (SRG) uses a continuous series of unitary transformations to decouple high-momentum and low-momentum physics in an input Hamiltonian [1, 2]. This decoupling means that expansions of physical observables generally become more convergent. The SRG can be implemented through a flow equation for the evolving Hamiltonian H_s,

$$\frac{dH_s}{ds} = [\eta_s, H_s] = [[G_s, H_s], H_s] , \qquad (1)$$

where s is a flow parameter [2, 3] and the generator η_s is specified by the operator G_s. With G_s chosen to be the relative kinetic energy $T_{\rm rel}$, the SRG has been applied successfully over the past few years to calculate nuclear structure and reactions [4–12]. However, different choices for G_s will give rise to different patterns of evolution, which may be advantageous. In this paper, two alternatives to $T_{\rm rel}$ are evaluated for their effectiveness in decoupling and, in particular, for improvements in computing speed (see Fig. 1 for a representative example). Our tests are for realistic nucleon-nucleon (NN) interactions in two-body systems and for a one-dimensional model Hamiltonian applied to few-body bound states.

We focus on novel generators that have G_s as functions of $T_{\rm rel}$. (Note: we can just as well consider the full kinetic energy T in our discussion, because the center-of-mass part commutes with the running Hamiltonian H_s, so we will use T for convenience.) In particular, we explore the "inverse" G_s operator

$$G_s = -\frac{\sigma^2}{1 + T/\sigma^2} \equiv G_s^{\rm inv} , \qquad (2)$$

and the "exponential" G_s given by

$$G_s = -\sigma^2 e^{-T/\sigma^2} \equiv G_s^{\rm exp} . \qquad (3)$$

Each has a Taylor series which reduces to T (up to a constant, which drops out from the commutator) at low
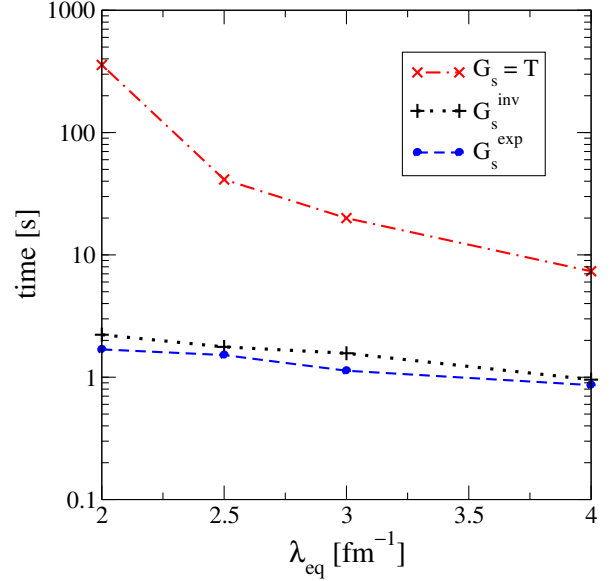
---

[*] li.1287@osu.edu

[†] anderson@physics.ohio-state.edu

[‡] furnstahl.1@osu.edu

FIG. 1. (color online) Computational time to evolve the Argonne v_{18} $^1S_0$ potential [13] as a function of the final value of $\lambda_{\rm eq}$ (see text) for several generators, with $\sigma = 2$ fm^{-1} for $G_s^{\rm inv}$ and $G_s^{\rm exp}$.

momentum or when σ is large. As such, the independent parameter σ controls the separation of a low-energy region where G_s behaves as T and the potential is driven towards the diagonal, and a high-energy region where evolution is suppressed. This suppression can result in a significant computational speedup of the SRG evolution when compared to calculations with $G_s = T$, while not impacting the advantageous properties of the evolution for low-momentum applications.

The suppression of running in unneeded parts of the Hamiltonian by the novel generators could mitigate the difficulties of evolving very large matrices for calculations of light atomic nuclei [11], opening the door to more tailored SRG generators and more effective evolution of three- and eventually four-body interactions. Even at the two-body level there are problems when trying to evolve to large values of the flow parameter s. A recent example is a study of SRG decoupling with large-cutoff effective field theory (EFT) potentials, which require evolution beyond the range usually considered [14]. In doing so,

the SRG differential equations can become extremely stiff and take a prohibitively long time (weeks on a single processor) to evolve. This problem has hindered exploratory studies into issues such as what happens when a chiral EFT is evolved to the regime of pionless EFT.

In Section II, we give representative results for applications to two-body systems, including an analysis of the flow pattern. These results are extended to few-body systems in Section III using a model one-dimensional Hamiltonian that has proved useful in past applications [15, 16]. We summarize and outline future studies in Section IV.

II.   TWO-NUCLEON SYSTEMS

In this section we give representative results for evolving realistic nucleon-nucleon potentials using the novel generators from Eqs. (2) and (3) in comparison to the usual choice of $G_s = T$.

A.   Performance

The key advantage of the novel generators that we wish to highlight is the improvement in computational performance. For example, the time needed to evolve the Argonne v_{18} $^1S_0$ potential [13] to equivalent levels of decoupling with several generators is plotted in Fig. 1. The parameter $\lambda \equiv 1/s^{1/4}$, which has dimensions of a momentum, has been used to identify the momentum decoupling scale. However, different generators will evolve a given potential at different rates, so comparing results with the same definition of λ can be misleading. Therefore, we identify an "equivalent" λ_{eq} for each novel generator that equalizes the degree of decoupling compared to $G_s = T$ (for which $\lambda_{eq} = \lambda$ by definition); the details are described in Section II B.

The value of σ will also have an impact, as discussed below; in Fig. 1 we use the intermediate value $\sigma = 2\,\text{fm}^{-1}$. With this choice, there is nearly an order of magnitude difference in the time to evolve the Argonne v_{18} potential with G_s^{exp} and G_s^{inv} compared to $G_s = T$ at $\lambda_{eq} = 4\,\text{fm}^{-1}$ and two orders of magnitude by $\lambda_{eq} = 2\,\text{fm}^{-1}$. Note that nuclear interactions have typically been evolved for nuclear structure studies to the range $\lambda = 1.5$–$2.2\,\text{fm}^{-1}$. The speed gains will depend on the initial potential and can be much less for the evolution of softer initial potentials; e.g., for the N3LO 500 MeV chiral EFT potential of Ref. [17], evolving with G_s^{exp} to $\lambda_{eq} = 2\,\text{fm}^{-1}$ is about 1.5 times as fast as with $G_s = T$ and about 3 times as fast to $\lambda_{eq} = 1.5\,\text{fm}^{-1}$.

The numerical solution of the SRG evolution equations requires repeated dense matrix-matrix multiplications. As a consequence, the evolution has been carried out on shared-memory computer architectures. Recent calculations using the SRG with many-body forces are approaching the limits of what is practical to evolve in memory on a single node due to the size of the model space needed [11]. A distributed scheme to solve the equations would permit larger model spaces to be utilized, however the dense matrix multiplication would then be limited by internode communication times. The reduced number of operations required by novel generators might help to make such a scheme possible.

B.   Decoupling and λ_{eq}

To validate the apparent computational advantages of the novel generators, one must confirm that the decoupling characteristics of the $G_s = T$ generator are also reproduced, so that calculations of physical observables also become more convergent. However, if we evolve to the same λ, the degree of decoupling for identical initial potentials differs for G_s^{exp} and G_s^{inv} compared to $G_s = T$. These differences are evident in the deviations of $^1S_0$ phase shifts calculated from the evolved potentials using G_s^{exp} and $G_s = T$ from the unevolved potential shown in Fig. 2 for several different λ values (only G_s^{exp} is shown; G_s^{inv} has a similar behavior). If the full potentials were used, the phase shifts would agree – up to numerical precision – with those from the initial potential, because the evolution in all cases is unitary. However, the degree of decoupling for a given value of λ can be made manifest by first cutting off the potential (that is, setting to zero its matrix elements) above some value of k and then calculating the phase shifts. In Fig. 2, for illustration, we choose the cutoff value k_{cut} to be $2\,\text{fm}^{-1}$. The signature
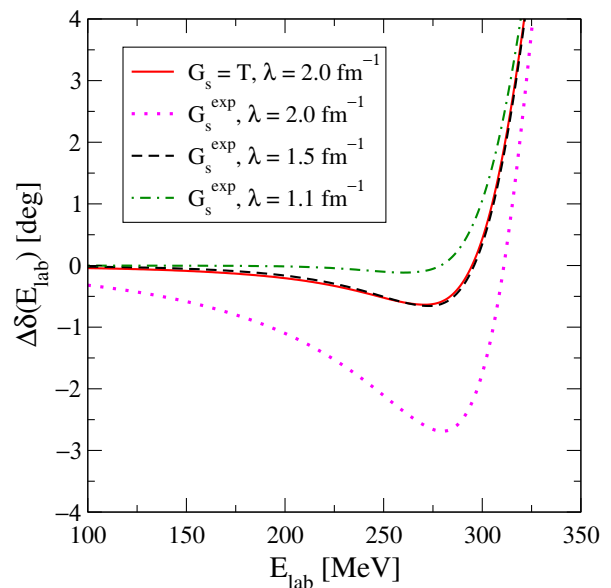

FIG. 2. (color online) Deviation of phase shifts calculated with the Argonne v_{18} $^1S_0$ potential [13] evolved with $G_s = T$ and G_s^{exp} ($\sigma = 2\,\text{fm}^{-1}$) to various λ values and then truncated at $k_{cut} = 2\,\text{fm}^{-1}$ to test decoupling. Phase shifts from untruncated potentials agree precisely with those from the initial potential.
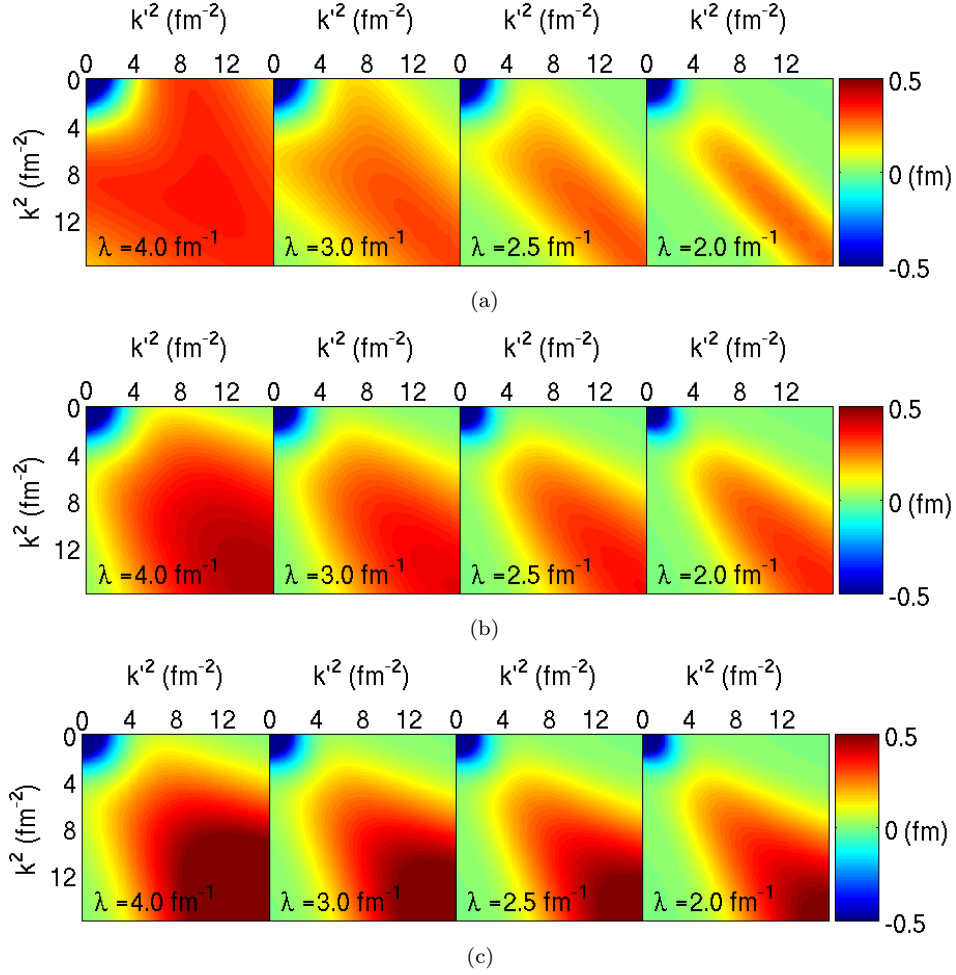
FIG. 3. (color online) Contour plots showing the evolution via Eq. (1) at several values of λ_{eq} starting from the momentum-space Argonne v_{18} $^1S_0$ potential [13] using (a) $G_s = T$; (b) G_s^{inv} from Eq. (2) with $\sigma = 2$ fm^{-1}; and (c) G_s^{exp} from Eq. (3) with $\sigma = 2$ fm^{-1}.

of decoupling is that the phase shifts agree at lower energies and only deviate close to and above the cutoff. This is typically observed when the potential is evolved so that λ is less than the cut momentum [18, 19].

This behavior provides us with a pragmatic way to define λ_{eq}, by identifying it with the decoupling behavior that is found for $G_s = T$ for a given λ. We use the results in Fig. 2 to illustrate the procedure. The continuous curve shows the deviation of phase shifts for the potential evolved with $G_s = T$ to $\lambda = 2$ fm^{-1} and cut at $k = 2$ fm^{-1}. As expected from decoupling, the deviation is small up to roughly k_{cut}. We use this level of agreement as the criterion for identifying equivalent λ's for other generators. That is, a potential is evolved to a series of λ values with a novel G_s and then cut at k_{cut} after evolution. The phase shifts are then compared to the level of decoupling observed for $G_s = T$ at $k_{\mathrm{cut}} = \lambda$. The approximate point in the novel G_s evolution for which the cut phase shifts agree is equated with λ_{eq}. Consider phase shifts for the potential evolved with G_s^{exp} to several

values of λ and cut at $k = 2$ fm^{-1}, as shown in Fig. 2. For G_s^{exp}, λ evolved to 1.5 fm^{-1} gives a similar degree of decoupling to λ evolved to 2 fm^{-1} with $G_s = T$. As a result, we define $\lambda = 1.5$ fm^{-1} to be the $\lambda_{\mathrm{eq}} = 2$ fm^{-1} for G_s^{exp}. We will use λ_{eq} below for most comparisons.

C. Flow Analysis

Having chosen a working definition for the decoupling scale of evolution with our novel generators, we can now take a closer look at the properties of the evolved potentials. In particular we would like to see how a potential flows with evolution using the novel generators compared to $G_s = T$, and to understand how the choice of σ affects this flow.

In Fig. 3 we compare the evolution pattern of the two-body potential in the $^1S_0$ channel with different generators. Each frame is a representation of the potential matrices in momentum space; where the matrix is
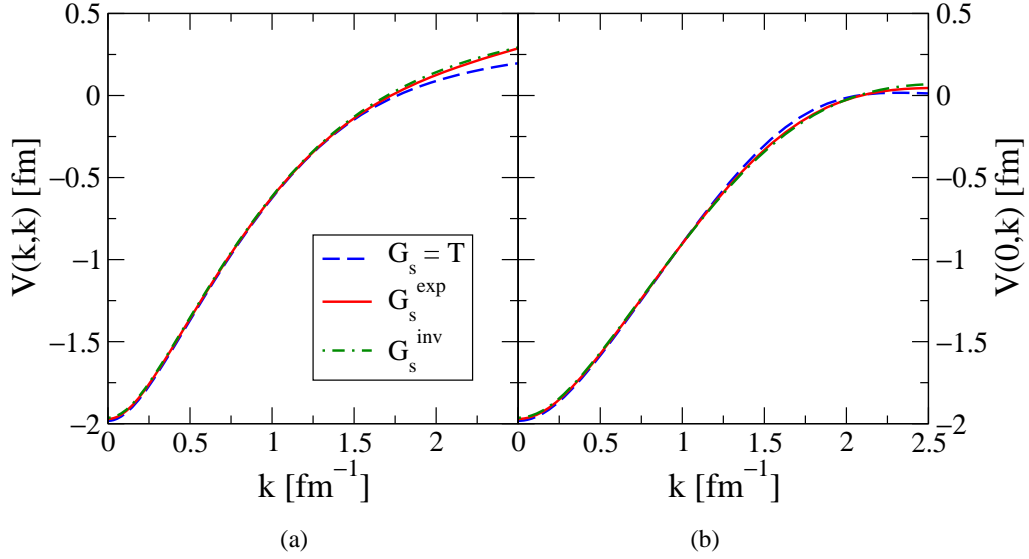
FIG. 4. (color online) Diagonal (a) and off-diagonal (b) momentum-space matrix elements for evolved Argonne v_{18} $^1S_0$ potential [13] with $G_s = T$ and novel generators G_s^{exp} and G_s^{inv} at $\lambda = 2\,\mathrm{fm}^{-1}$ with $\sigma = 2\,\mathrm{fm}^{-1}$.
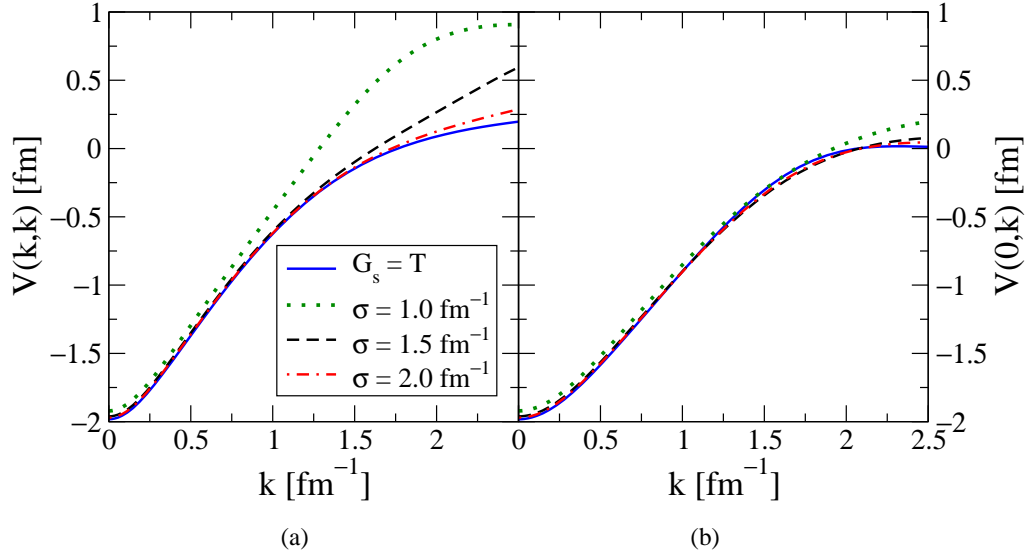

FIG. 5. (color online) Diagonal (a) and off-diagonal (b) momentum-space matrix elements for evolved Argonne v_{18} $^1S_0$ potential [13] with $G_s = T$ and G_s^{exp} with different values of σ each evolved to $\lambda = 2\,\mathrm{fm}^{-1}$. The lines with $\sigma = 3\,\mathrm{fm}^{-1}$ are indistinguishable from the ones with $G_s = T$.

zero, there is no coupling between momentum components. The initial potential in all cases is Argonne v_{18} [13] and the value of σ is taken to be $2\,\mathrm{fm}^{-1}$. Note that at $\lambda = 4\,\mathrm{fm}^{-1}$, the first matrix plotted here, there is already significant evolution. As the potential is evolved, its high and low momentum components become increasingly decoupled, as expected. It is evident that the evolved potentials are similar (but not identical) in the region where $k^2, k'^2 < \sigma^2$. When $\lambda < \sigma$ we find that σ roughly defines the low momentum region where the novel generators behave as $G_s = T$. The minor differences in this low momentum region can be attributed to the fact that the

point in evolution, λ, needed for the novel generators to reach the corresponding λ_{eq} occurs when $\lambda < \lambda_{\mathrm{eq}}$. At higher momenta, novel generator evolution is suppressed relative to $G_s = T$. The patterns here are characteristic of the particular generator and are similar for other potentials and in other channels.

This nature of the evolution is further illustrated by the plots in Figs. 4 and 5, which show a detailed view of the diagonal and off-diagonal values of the matrices at low momentum for each generator applied to the Argonne v_{18} $^1S_0$ potential . The flow parameter was run to $\lambda = 2\,\mathrm{fm}^{-1}$ with the generators here to distinguish be-
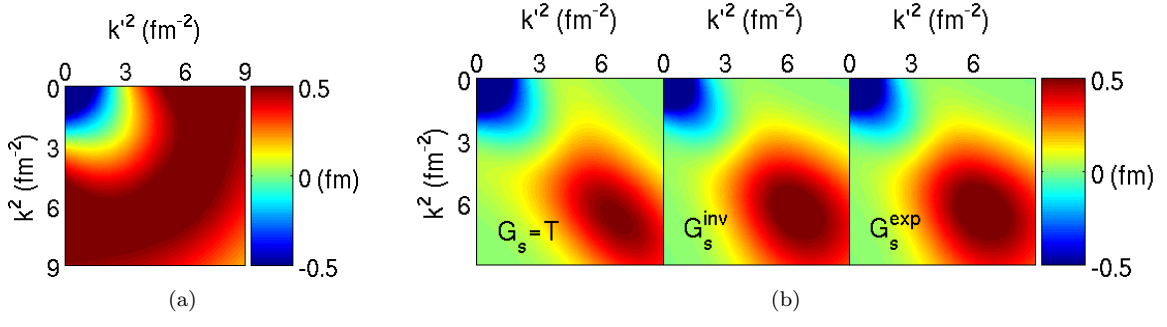
FIG. 6. (color online) (a) Unevolved N^{3}LO 500 MeV ^{1}S$_0$ potential . (b) Contour plot showing the evolved N^{3}LO ^{1}S$_0$ potential with different generators to $\lambda_{\mathrm{eq}} = 2\,\mathrm{fm}^{-1}$. For G_s^{exp} and G_s^{inv}, $\sigma = 2\,\mathrm{fm}^{-1}$.
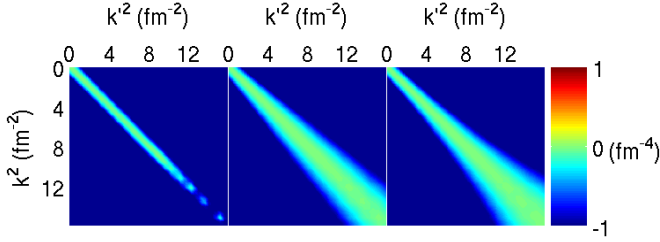

FIG. 7. (color online) Color contour plots of the first term (excluding the factor due to V_s) on the right side of Eq. (6) for $G_s = T$ (left), G_s^{inv} (middle), and G_s^{exp} (right). The last two use $\sigma = 2\,\mathrm{fm}^{-1}$.
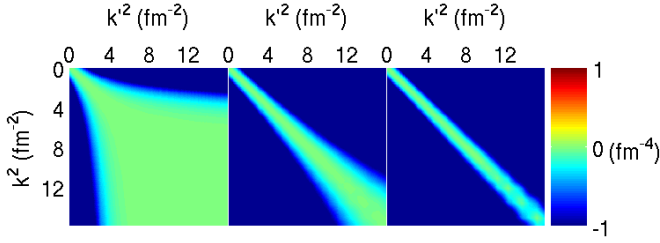

FIG. 8. (color online) Color contour plots of the first terms (excluding the factor due to V_s) on the right side of Eq. (6) for G_s^{exp} with $\sigma = 1, 2$, and $3\,\mathrm{fm}^{-1}$ from left to right.

tween ambiguities caused by using λ_{eq}. In Fig. 4, the values from different generators agree quite well for $k < \sigma$, where $\sigma \approx \lambda$. Moreover, we see that the minor "pincushion" effect seen in Fig. 3 for the novel generators relative to $G_s = T$ is indeed an artifact of using λ_{eq}, as each curve falls to zero at approximately the same time. In Fig. 5 we focus on G_s^{exp} versus $G_s = T$ and the fact that they differ for $\sigma \le \lambda$. But, as $\sigma \to \lambda$ it is evident that the evolution of the novel generator becomes increasingly similar to $G_s = T$ in the low-momentum region $k < \lambda$. For larger values of σ the novel generators become indistinguishable from $G_s = T$.

As a demonstration of similar behavior for different NN potentials, an evolved potential with different generators in the ^{1}S$_0$ channel of the N^{3}LO 500 MeV potential [17]

is shown in Fig. 6. Note that the initial potential has significantly less coupling at high momentum compared to Argonne v_{18} [8]. As a result, there is correspondingly less improvement in evolution speed. However, the general features of the evolution patterns with different generators seen with Argonne v_{18} are also seen for the N^{3}LO potential.

To better understand the evolution process, we need to look further into the flow equation itself. Evaluating Eq. (1) in a two-body partial-wave momentum space basis with $G_s = T$ yields

$$
\frac{dV_s(k,k')}{ds} = -(k^2 - k'^2)^2 V_s(k,k')
$$
$$
+ \frac{2}{\pi} \int_0^\infty q^2 dq \,(k^2 + k'^2 - 2q^2) V_s(k,q) V_s(q,k') . \quad (4)
$$

In the far off-diagonal region, the first term dominates (this is true for the ordinary range of λ but is modified when λ is comparable to the binding momentum of a bound state). This implies that each off-diagonal matrix element is driven to zero as

$$
V_s(k,k') \xrightarrow{k \ne k'} V_{s=0}(k,k')\, e^{-s(k^2 - k'^2)^2} . \quad (5)
$$

For $G_s = f(T)$, these results are modified to

$$
\frac{dV_s(k,k')}{ds} = -\big(k^2 - k'^2\big)\big(f(k^2) - f(k'^2)\big) V_s(k,k')
$$
$$
+ \frac{2}{\pi} \int_0^\infty q^2 dq \,\big(f(k^2) + f(k'^2) - 2f(q^2)\big)
$$
$$
\times V_s(k,q) V_s(q,k') . \quad (6)
$$

and

$$
V_s(k,k') \xrightarrow{k \ne k'} V_{s=0}(k,k')\, e^{-s(k^2 - k'^2)(f(k^2) - f(k'^2))} . \quad (7)
$$

The difference in the exponents of Eqs. (5) and (7) for $k \sim \lambda$ leads to $\lambda_{\mathrm{eq}} < \lambda$.

The first term of the flow equation (excluding the factor due to the potential) for each of our generators is shown as a contour plot in Figs. 7 and 8. In Fig. 7 we see that T works uniformly (in k^2) on the entire region
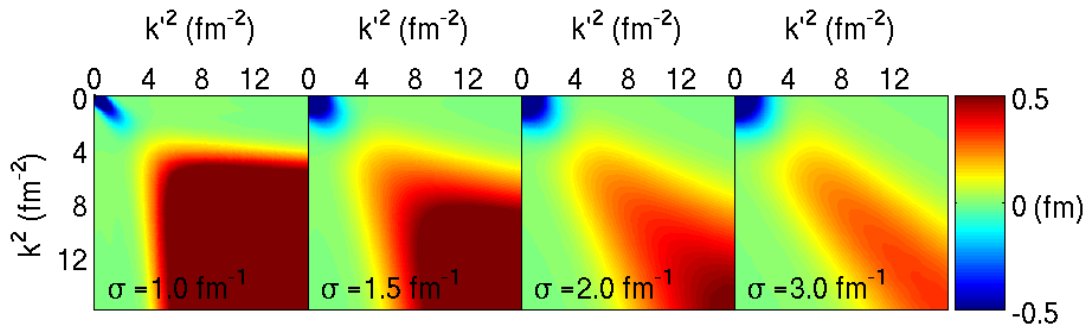
FIG. 9. (color online) Contour plot showing the evolution to $\lambda_{\mathrm{eq}} = 2\,\mathrm{fm}^{-1}$ via Eq. (1) starting from the momentum-space Argonne v_{18} $^1S_0$ potential [13] using G_s^{exp} from Eq. (3) with different values of σ.
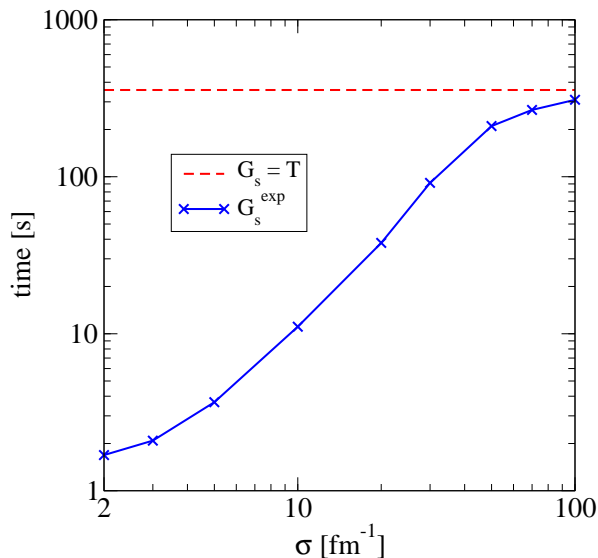

FIG. 10. (color online) Computational time to evolve the Argonne v_{18} $^1S_0$ potential [13] with $G_s = T$ and G_s^{exp} to $\lambda_{\mathrm{eq}} = 2\,\mathrm{fm}^{-1}$ as a function of the value of σ.

given decoupling parameter λ_{eq} should be less for G_s^{inv} or G_s^{exp} than for $G_s = T$. The dramatic drop in evolution time seen in Fig. 1 for the novel generators makes it apparent that they are more efficient. However, we can also look at how the choice of σ affects their performance. This is shown in Fig. 10 for G_s^{exp}, where we see that the time spent evolving to $\lambda_{\mathrm{eq}} = 2$ fm^{-1} decreases as σ decreases. As σ becomes smaller, the evolution at high momentum is increasingly limited, which we correlate with improvement in computation time; as σ increases, the evolution time approaches that of T (as does the flow). Note that for the Argonne v_{18} potential a large σ is needed before G_s is effectively equal to T.

In practical applications, one might optimize the trade-off between decoupling and computational speedup by choosing σ to be approximately equal to, or slightly greater than the λ corresponding to λ_{eq}. Then the decoupling properties of $G_s = T$ are preserved in the low momentum region of interest while still enhancing the computational performance of the evolution by limiting the evolution at high momentum. However, this prescription has not yet been tested in detail.

of the potential. With G_s^{inv}, there is much less evolution close to the diagonal. The plot for G_s^{exp} is similar, but exhibits even less evolution in the middle region.

It is evident here that the novel generators will result in less evolution at high momenta, as we have seen, and that this should be a generic result for other partial waves and for higher-body evolution, because it depends only on kinetic energy differences. We also see how the value of σ controls the degree to which the operator G_s is similar to T. This is illustrated in Fig. 8. If $\sigma = 1$ fm^{-1}, only the edges of the potential are modified; the shape is completely different from T. For $\sigma = 3$ fm^{-1}, there is the thinnest band on the diagonal, which is closest to T. At very large σ, there is a transition to T. In the plots of Fig. 9 we see how the final evolved flow is affected by differing choices of σ.

The limited evolution at high momenta seen in the novel generators suggests that the time to evolve to a

III. FEW-BODY TESTS IN A ONE-DIMENSIONAL MODEL

The effects on matrices in a momentum basis demonstrated in the last section are generic and so should carry over to alternative bases and to higher-body forces. Calculations for realistic three-dimensional few-body systems are not yet available, but we can test the generators in a one-dimensional model of bosons that has proven to accurately predict the evolution of three-dimensional few-body forces [15]. The model we use was originally introduced in Ref. [20] as a sum of two gaussians to simulate repulsive short-range and attractive mid-range nucleon-nucleon two-body potentials. It is written in coordinate space as

$$V^{(2)}(x) = \frac{V_1}{\sigma_1\sqrt{\pi}}e^{-x^2/\sigma_1^2} + \frac{V_2}{\sigma_2\sqrt{\pi}}e^{-x^2/\sigma_2^2} \qquad (8)$$

Basis	Momentum	Oscillator		
System	$A = 2$	$A = 2$	$A = 3$	$A = 4$
$\sigma = 2$	3.3	3.3	3.8	4.1
$\sigma = 3$	2.6	2.6	2.7	2.8

TABLE I. Speed up in model A-particle 1D oscillator basis for evolution to $\lambda_{eq} \approx 3$, comparing the ratio of the time to evolve $G_s = T$ versus G_s^{exp}. The results for G_s^{inv} are very similar.

or in momentum space as

$$V^{(2)}(p, p') = \frac{V_1}{2\pi\sqrt{2}} e^{-(p-p')^2 \sigma_1^2/8} + \frac{V_2}{2\pi\sqrt{2}} e^{-(p-p')^2 \sigma_2^2/8} , \tag{9}$$

where $V_1 = 12$, $\sigma_1 = 0.2$, $V_2 = -12$, and $\sigma_2 = 0.8$ (see Ref. [20] for discussion of units). Also, in calculations with an initial three-body potential, a regulated contact interaction is used. This is written as

$$V^{(3)}(p, q, p', q') = c_E \, f_\Lambda(p, q) f_\Lambda(p', q'), \tag{10}$$

where c_E corresponds to the strength of the interaction, and

$$f_\Lambda(p, q) = e^{-((p^2+q^2)/\Lambda^2)^n}. \tag{11}$$

The regulator cutoff $\Lambda = 2$, and the sharpness of the fall-off is set to $n = 4$. We have chosen these parameters for comparison with Ref. [15].

A. Performance

Our first test is to confirm that the enhanced computational performance characteristics of the novel generators are maintained in the few-body basis. Table I shows the speedup obtained using the G_s^{exp} generator with the model potential described above. The performance of the G_s^{inv} generator is very similar to the G_s^{exp} results quoted here. Results are reported at an optimal λ_{eq}; we do not use a range of λ values here due to particularities of the oscillator basis convergence properties, as will be discussed in more detail below.

What we find is that the evolution of the two-body force in 2-, 3-, and 4-particle systems with novel generators are all 2.5–4 times faster than the evolution with $G_s = T$ (to the same degree of decoupling). The performance enhancement is relatively basis independent, with the speedup for the momentum and oscillator bases found to be roughly equivalent. While the speedup improvement is much smaller than found for Argonne v_{18}, we do not expect a direct correspondence. The important point is that the speedup in the A=2 particle system serves as a good predictor of the speedup in the A=3 and 4 systems. So one might expect a similar improvement in few-body oscillator basis calculations with Argonne v_{18} as found above for Argonne v_{18} in the 2-particle partial-wave momentum basis. This will be significant as we move to novel generator calculations in realistic three-dimensional systems.

B. Decoupling

The measure of performance using the novel generators depends explicitly on their decoupling properties in the few-body harmonic oscillator basis relative to $G_s = T$. Ultimately, we find the level of decoupling obtained with $G_s = T$ to be matched by the novel generators.

However, the convergence properties of the oscillator basis with respect to SRG evolution, and consequently the issue of selecting an appropriate λ_{eq} in this basis, is more complicated than for the momentum basis. The convergence of observables depends on a balance of the ultraviolet (UV) and infrared (IR) cutoffs intrinsic to the choice of a particular oscillator basis. These cutoffs are given by [11]

$$\Lambda_{\mathrm{UV}} \sim \sqrt{m N_{\mathrm{max}} \hbar \Omega} \tag{12}$$

and

$$\Lambda_{\mathrm{IR}} \sim \sqrt{\frac{m\hbar\Omega}{N_{\mathrm{max}}}} , \tag{13}$$

where Ω is the oscillator frequency, and N_{max} is the maximum number of total oscillator excitations in the basis. Thus, a cutoff in oscillator basis states results in two approximate cutoffs in momentum space. But the SRG, using the generators being considered here, only provides a means to effectively lower the UV cutoff (by decoupling high and low momentum degrees of freedom in the Hamiltonian). As such, convergence is not monotonically improved with respect to evolution in λ.

As a measure of the decoupling, we plot the binding energy of the lowest energy state for an A-particle system with respect to N_{cut} for evolutions of the initial Hamiltonian to various λ (this procedure was carried out for $G_s = T$ using this model in [15]). The actual calculation is carried out by evolving the model interaction to λ in an initial basis large enough so that the binding energy is well converged. The Hamiltonian is then truncated at N_{cut} and the binding energies calculated in the reduced basis. The value of N_{cut} refers to the number of oscillator excitations in the basis, and is the oscillator basis equivalent of the k_{cut} parameter in momentum space, as used in Sec. II. But again, each N_{cut} here corresponds to a rough Λ_{UV} and Λ_{IR} truncation in momentum space.

Results are shown in Fig. 11 for the A = 2-, 3-, and 4-particle systems using G_s^{exp} with $\sigma = 3$ for selected values of λ. The signature of decoupling is the improved convergence of the binding energy at smaller N_{cut} with respected to SRG evolution. As the interaction is evolved the degree of decoupling gets better. This is only true up to some value of λ, however, at which point the degree of decoupling starts to get worse. It is the latter behavior which is introduced by the IR cutoff of the oscillator basis
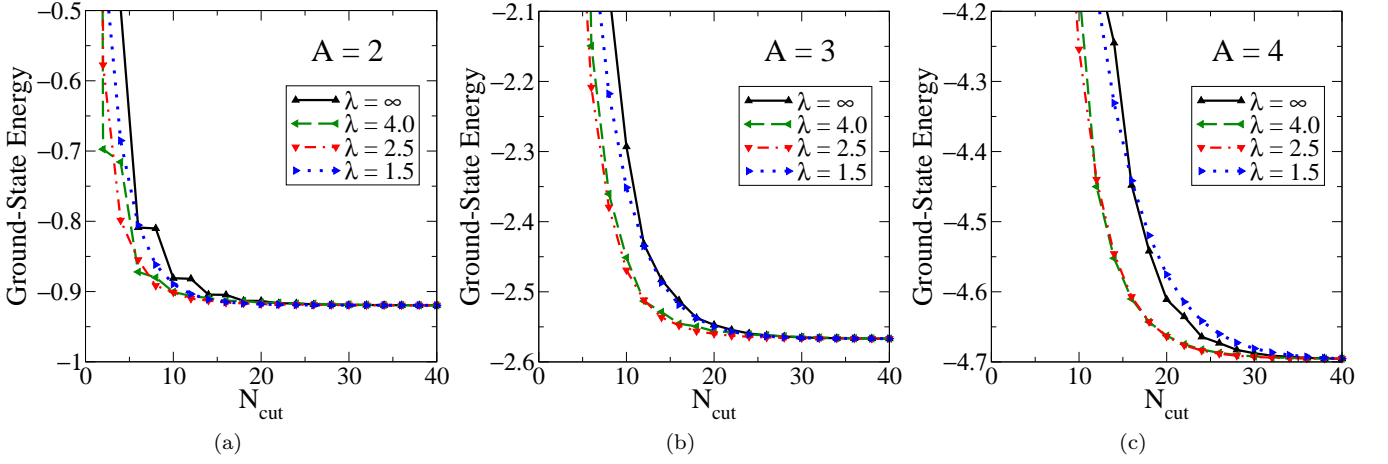
FIG. 11. (color online) Decoupling using $G_s^{\exp}$ with $\sigma = 3$ for (a) $A = 2$, (b) $A = 3$, and (c) $A = 4$. The initial two-body only potential is evolved to each λ shown in a basis with $N_{\max} = 40$. Matrix elements of the potential are set to zero if one or both states have $N > N_{\mathrm{cut}}$ and the resulting Hamiltonian is diagonalized to obtain the ground-state energies plotted.
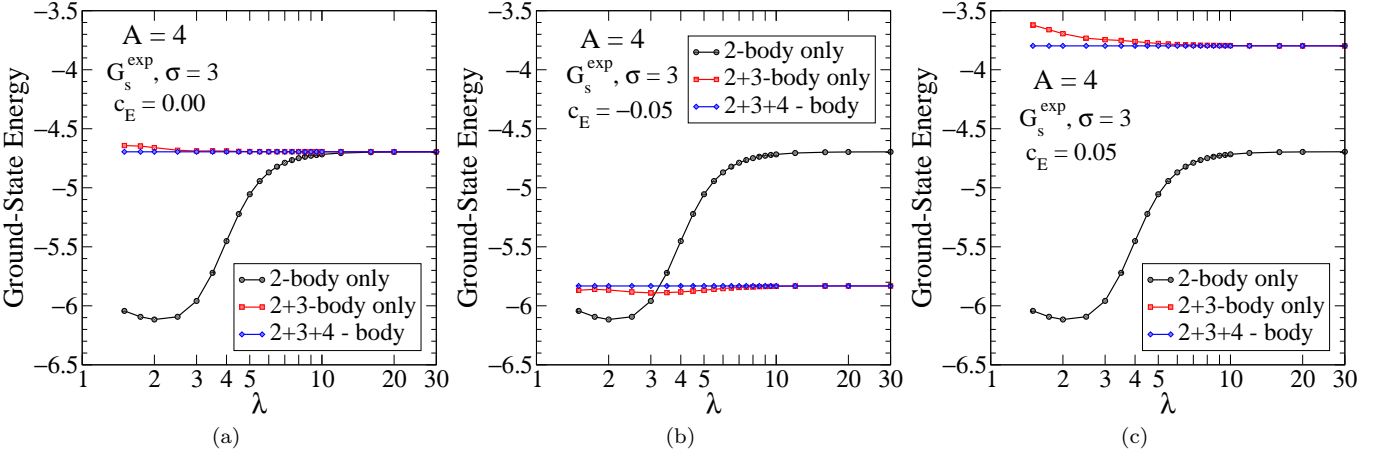

FIG. 12. (color online) The lowest bound-state energy for a four-particle system as a function of λ evolved using the SRG $G_s^{\exp}$ generator and an $N_{\max} = 40$ basis with an initial three-body potential with strength (a) $c_E = 0.0$, (b) $c_E = -0.05$, and (c) $c_E = 0.05$. The (blue) curves with diamonds include the full evolution of the Hamiltonian while the (black) curves with circles use the two-body potential evolved in the two-particle system and the (red) curves with squares use the two- and three-body potential evolved in the three-particle system. Evolution with G_s^{inv} is almost indistinguishable.

that complicates our efforts to choose a λ_{eq}, since a one-to-one correspondence with λ is no longer clear.

Nevertheless, a practical choice can be made by equating the λ with λ_{eq} when decoupling is found to be optimal in the $G_s = T$ and novel generator evolutions. The optimal levels of evolution happen to coincide at $\lambda \approx 3$ for $G_s = T$ and the novel generators. Thus, the speedup results in Table I were reported at $\lambda_{\mathrm{eq}} = 3$. Moreover, given these values for λ and λ_{eq}, we have chosen $\sigma = 3$ for most of the model space calculations in this section.

One may note that differences do exist between the $G_s = T$ and novel generator decoupling results, particularly at low N_{cut} [15]. However, the level at which any of the generators become well converged to the exact results with respect to N_{cut} are effectively the same. Thus, it is reasonable to make the comparisons we have done here

in order to determine λ_{eq}.

C. Induced Many-Body Forces

In general, the evolution of an interaction via the SRG leads to induced many-body forces. This is evident if we examine the second quantized form of the Hamiltonian

$$H = T_{ij} a_i^\dagger a_j + V_{ijkl} a_i^\dagger a_j^\dagger a_l a_k + \cdots \qquad (14)$$

where the dots indicate that higher-body forces may also be present in the initial interaction. When the SRG commutators in Eq. (1) are performed, one can see that many-body forces will be induced. These induced forces could pose a serious problem for few-body calculations

because at some point we must truncate the model space in numerical calculations, which will alter the predicted value of observables. These can be controlled, however, if there is a hierarchy of many-body forces so that successively larger many-body components are suppressed, and one can include at most one or two induced pieces to obtain well converged results. This has been found to be the case for $G_s = T$ and needs to hold for any practical alternative generators.

A measure of the induced many-body forces (which has been used in previous studies [6, 11, 15]) is to calculate the ground state energies of the $A = 3$ and 4 particle systems starting with a 2-body interaction and to examine how this energy changes with and without the induced 3- and 4-body components, as a function of the evolution parameter λ. We do this in Fig. 12 with a plot of the ground-state energy for the 4-particle system with the initial 2-body interaction embedded and evolved in the $A = 2$-, 3- and 4-body bases with novel generators G_s^{exp}. The results for G_s^{inv} are virtually indistinguishable. The curves show that the hierarchy of induced many-body forces is preserved for the novel generators just as with $G_s = T$ [15] (see, however, Ref. [21]). This hierarchy also holds for calculations with an initial three-body force and in the $A = 3$ particle system.

In summary, the model results suggest that the advantageous features of SRG evolution with $G_s = T$ can be maintained with the added computational performance of the novel generators when applied to realistic three-dimensional few-body calculations.

IV. SUMMARY

In this work, novel generators for the SRG that are functions of the kinetic energy operator T with an adjustable scale parameter σ were tested. We found that functions which reduce to T for basis states with kinetic energy less than σ preserved the good features of T, such as decoupling, but efficiently suppressed evolution for higher kinetic energies and thereby took much less time to evolve. Specific examples were considered, but other choices with a Taylor expansion starting with T should give comparable results. Their action was understood using a simple analysis of how the generators directly affect regions of high and low momentum. If σ is taken large enough, the generators become equivalent to T. It is important to note that not only the two-body properties of T were preserved by the novel generators, but also its characteristics in a few-body model space. This includes decoupling and the hierarchy of induced many-body forces, which is critical for applications to larger systems of particles.

The novel generators allow us to evolve potentials to much smaller values of λ than previously feasible. This should enable us to explore the transition between pionful and pionless regions of EFT potentials and further test the observations of Glazek and Perry about evolving past a bound state [22]. The original choice for G_s advocated by Wegner and collaborators [2, 3] and applied extensively in condensed matter is the diagonal component of the interaction, $G_s = H_{\text{diag}}(s)$,

$$\langle i|H_{\text{diag}}(s)|j\rangle \equiv \begin{cases} \langle i|H(s)|j\rangle & \text{if } i = j \, , \\ 0 & \text{otherwise.} \end{cases} \tag{15}$$

In Ref. [22], it was observed that when evolving a simple model past a bound state the Wegner evolution with H_{diag} will decouple the bound state by leaving it as a delta function on the diagonal of the Hamiltonian. In contrast, with $G_s = T$ the bound states remained coupled to low-momentum, and were pushed to the lowest momentum part of the matrix. This behavior was explored in Ref. [14] for leading-order, large-cutoff EFT potentials featuring deeply bound spurious states. However, it has not been studied for the physical deuteron state, which requires evolving well below $\lambda = 1$ fm^{-1}. This is now easily possible with the replacement of H_{diag} for T in Eqs. (2) and (3), although there are as-yet-unsolved complications from the discretization of the momentum basis.

The most important next step for the novel generators is to apply them to evolve realistic few-body potentials, where speeding up the evolution is desirable due to the large sizes of the matrices involved. The novel generators can be applied directly to few-particle bases using the method described in Refs. [6, 11, 15]. Calculations in a one-dimensional model performed here imply that the speed-up carries over to three-body forces and could have a significant impact in making realistic calculations with additional induced many-body forces feasible.

ACKNOWLEDGMENTS

[1] S. D. Glazek and K. G. Wilson, Phys. Rev. D **48**, 5863 (1993).

[2] F. Wegner, Ann. Phys. (Leipzig) **3**, 77 (1994).

[3] S. Kehrein, *The Flow Equation Approach to Many-*

Particle Systems (Springer, Berlin, 2006).

[4] S. K. Bogner, R. J. Furnstahl, and R. J. Perry, Phys. Rev. C **75**, 061001 (2007).

[5] S. K. Bogner *et al.*, Nucl. Phys. A **801**, 21 (2008).

[6] E. D. Jurgenson, P. Navratil, and R. J. Furnstahl, Phys. Rev. Lett. **103**, 082501 (2009).

[7] S. K. Bogner, R. J. Furnstahl, A. Nogga, and A. Schwenk, arXiv:0903.3366 [nucl-th].

[8] S. K. Bogner, R. J. Furnstahl, and A. Schwenk, Prog. Part. Nucl. Phys. **65**, 94 (2010).

[9] P. Navratil, R. Roth, and S. Quaglioni, Phys. Rev. C **82**, 034609 (2010).

[10] P. Navratil, S. Quaglioni, and R. Roth, (2010), arXiv:1009.3965 [nucl-th].

[11] E. Jurgenson, P. Navratil, and R. Furnstahl, Phys. Rev. C **83**, 034301 (2011).

[12] H. Hergert, P. Papakonstantinou, and R. Roth, Phys. Rev. C **83**, 064317 (2011).

[13] R. B. Wiringa, V. G. J. Stoks, and R. Schiavilla, Phys. Rev. C **51**, 38 (1995).

[14] K. Wendt, R. Furnstahl, and R. Perry, Phys. Rev. C **83**, 034005 (2011).

[15] E. D. Jurgenson and R. J. Furnstahl, Nucl. Phys. A **818**, 152 (2009).

[16] E. R. Anderson, S. K. Bogner, R. J. Furnstahl, and R. J. Perry, Phys. Rev. C **82**, 054001 (2010).

[17] D. R. Entem and R. Machleidt, Phys. Rev. C **68**, 041001 (2003).

[18] E. D. Jurgenson, S. K. Bogner, R. J. Furnstahl, and R. J. Perry, Phys. Rev. C **78**, 014003 (2008).

[19] S. K. Bogner, R. J. Furnstahl, R. J. Perry, and A. Schwenk, Phys. Lett. B **649**, 488 (2007).

[20] C. Alexandrou, J. Myczkowski, and J. W. Negele, Phys. Rev. C **39**, 1076 (1989).

[21] R. Roth, J. Langhammer, A. Calci, S. Binder, and P. Navratil, Phys. Rev. Lett. **107**, 072501 (2011).

[22] S. D. Glazek and R. J. Perry, Phys. Rev. D **78**, 045011 (2008).